INDIAN JOURNAL OF SCIENCE AND TECHNOLOGY

ORIGINAL RESEARCH

OPEN ACCESS

Received: 13/11/2025

Accepted: 04/02/2025

Published: 08/04/2025

Citation: Tankasala V, Kavitha G, Vittal C, Dhanalaxmi V, Padma P (2025) Effect of MHD on Chemically Retorting Oldroyed-B + Nanofluid Flow Over a Stretching Sheet Through Porous Medium in the Presence of Double Diffusion. Indian Journal of Science and Technology 18(12): 947-961. https://doi.org/10.17485/IJST/v18i12.3697

* **Corresponding author**.

Tel: 9966998024
vijaya9966998024@rediffmail.com

Funding: None

Competing Interests: None

Published By Indian Society for Education and Environment (iSee)

ISSN
Print: 0974-6846
Electronic: 0974-5645

Effect of MHD on Chemically Retorting Oldroyed-B + Nanofluid Flow Over a Stretching Sheet Through Porous Medium in the Presence of Double Diffusion

Vijayalaxmi Tankasala[1]*, G Kavitha[2], Ch Vittal[3], V Dhanalaxmi[2], P Padma[4]

1 Department of Mathematics, Government Degree College, Shadnagar, Ranga Reddy, Telangana State, India, Tel.: 9966998024
2 Department of Mathematics, University College of Science, Osmania University, Hyderabad, Telangana State, India
3 Department of Mathematics, University College of Science, Saifabad, Osmania University, Hyderabad, Telangana State, India
4 Padma, Department of Mathematics, Government Degree College, Paloncha, Bhadradri Kottagudem, Telangana State, India

Abstract

Objectives: To investigate the combined effects of thermal diffusion and diffusion thermo on two-dimensional, steady, incompressible, viscous, electrically conducting, chemically reacting Oldroyd-B + nanofluid flow through a porous medium near a stretching sheet under the influence of a magnetic field. **Method:** We convert the main governing equations, which are a set of nonlinear partial differential equations, into sets of nonlinear ordinary differentials representing the motion, energy, and concentration of nanofluids as well as the boundary conditions via similarity transformations. The implicit finite element method is utilized to solve these equations numerically. **Findings:** The main findings are the heat transfer rate is rising with growing values of Nb, Nt, Du, while it reducing for increasing values of Pr and Le also the mass transfer rate is growing with higher values of Nt, and Sr, and the reverse effects is observed in case of increasing values of Le, Nb and δ. **Novelty:** Investigating the significance of MHD Oldroyd-B + nanofluid flow past a stretched sheet through a porous media with chemical reaction is the novel aspect of this work. The effects of thermophoresis and Brownian motion are two essential elements as well as the effects of magnetic fields, Soret, and Dufour are taken into account.

Keywords: OldroydB Fluid; Nanofluid; Chemical Reaction; MHD; Double Diffusion; Finite Element Method

1 Introduction

A study conducted by Hussain and colleagues [1] brought to light the relevance of nanometer-sized particles in contemporary technology, namely in terms of enhancing the electrical properties of various kinds of fluids. Li et al. [2] proposed the extensive use of mass transportation with activation power in a variety of important disciplines, such as hydropower engineering, chemistry, petroleum droplets, and food processing. According to Thejas et al. [3], nanotechnology, which is defined as the manipulation of matter on a very small scale, is used in a variety of fields, including chemical engineering, materials research, biological sciences, and healthcare. Ahmed et al. [4] conducted research on a number of nanomaterials, including carbon nanotubes, metal oxides, nanoscale polymers, and nanoscale clays, all of which are known for possessing excellent thermophysical characteristics. By increasing the injection parameter and the Eckert number, Aly [5] proposed that graphene nanoparticles could perform the functions of a heater and a cooler. Additionally, by increasing both the first and second velocity slips, they could perform the role of a cooler. In order to improve heat transfer in a hybrid nanofluid mixture of non-magnetic and magnetic nanoparticles based on sodium alginate, Hussanan and his colleagues [6] performed research according to the following methodology. During their research, Arshad Khan and his colleagues [7] investigated the development of entropy and carried out thermal analysis on the rotational motion of a hydromagnetic Casson nanofluid that was contained inside a spinning vessel that was heated by Joules. Khan and colleagues [8] investigated the transport of heat and mass in a three-dimensional nanofluid flow that was carried out on a linear stretching surface with convective boundary conditions. The researchers Manna et al. [9] investigated the influence that the position of hot chillers and the Lorentz effect had on the transmission of heat and the creation of energy in a cavity that was quarter-circular in shape and contained hybrid nanofluid convection. Waqas et al. [10] conducted an analysis of the results of a computer model about the impacts of biological convection on the magnetohydrodynamics flow of nanofluids inside a framework that might be described as horizontally expanding and rotating. Research conducted by Waqas and colleagues [11] investigated the effect that magnetohydrodynamics radiation had on the movement of a hybrid nanofluid over a spinning disk. Lu et al. [12] carried out a numerical investigation on a fluid flow consisting of three layers, one of which was a nanoparticle layer. In a three-layer model, Rajeev et al. [13] investigated the phenomenon of cross-diffusion in a sinusoidal channel for the flow of a hybrid nanofluid that was surrounded by single-phase nanofluids. The effects of Hall currents and Ohmic heating were taken into consideration in the research conducted by Abbasi and colleagues [14] about the entropy generation analysis of the peristaltic motion of nanofluid in a symmetric channel. A comparative analysis of the efficiency of heat transmission was carried out by Ma et al. [15] for a number of nanofluids that had varying mass concentrations. Research conducted by K. Gangadhar et al. [16] investigated the Oldroyd-B flow of nanofluid over a stretched surface that included gyrotactic microorganisms. The researchers took into account effects such as the Lorentz force. In their study, Rafiq and colleagues [17] investigated the peristalsis of a viscous nanofluid in a channel wall that was flexible. They took into consideration ion-slip, strong magnetic field, Hall current, thermophoresis, and Brownian motion occurrences. Hina et al. [18] used the Buongiorno model in order to investigate the peristaltic movement of a Carreau–Yasuda nanofluid while it was flowing in a symmetrical channel. Using Powell-Eyring nanofluid, Tanveer and Malik [19] investigated the inclusion of a number of parameters in a curved geometry flow with MHD peristalsis. These components included thermo-diffusion, changing viscosity, viscous dissipation, porosity, and slip. The physical consequences of magnetohydrodynamic (MHD) effects on Oldroyd-B nanofluids are substantial in a variety of real-world applications, especially in sectors where fluids must transport heat efficiently while being exposed to magnetic fields. Since nanofluids frequently display shear thinning or viscoelastic characteristics, which qualify them for sophisticated heat transfer procedures, the Oldroyd-B model, which characterizes non-Newtonian fluid behavior, is pertinent to them. Through modifications to viscosity, velocity profiles, and heat conduction, MHD effects impact the flow behavior of nanofluids when a magnetic field is applied. Because of their improved heat transfer capabilities, nanofluids with MHD effects can enhance thermal performance in real-world applications such as heat exchangers, cooling systems, and nuclear reactors. Better conductivity is provided by the fluid's nanoparticles, and the fluid's velocity is altered by the magnetic field, which results in. A study conducted by Rafiq and colleagues [20] examined the electro-osmotic magnetohydrodynamic peristaltic flow of Jeffrey nanofluid in a curved geometry, taking into account the presence of chemical reaction and slip conditions. Khyati Dang et al. studied the chemical effect on Mathematical Simulation for MHD Casson Convective Nanofluid Flow Induced by 3D Permeable Sheet [21] and also investigated the effect of MHD on radiative Casson Non-Newtonian Nanofluid slip flow induced by stretching cylinder [22]. Finally, Amith et al. studied the effect of slips and MHD on the melting fluid flow of Oldroyd-B + nanofluid [23] and Ali and co-authors delve effect of heat and mass transfer of Oldroyd-B + nanofluid flow in a porous medium [24]. With motivation of the above work is to investigate the importance of MHD Oldroyd-B + nanofluid flow past a stretched sheet through a porous medium with a chemical reaction. In many applications, the behavior of Oldroyd-B nanofluids is influenced by double diffusion, where fluid flow is influenced by both concentration and temperature gradients. The Oldroyd-B model's non-Newtonian characteristics, which take into account the fluid's elastic and viscous components, combine with heat and mass transfer to produce the double diffusion process, especially in nanofluids.Double diffusion may occasionally improve Oldroyd-B nanofluid flow properties. The interplay between thermal and concentration gradients, for instance, might increase the overall efficiency of heat and mass transfer in cooling systems or heat exchangers. Better flow management and more effective heat dissipation result from the fluid's nanoparticles' enhancement of thermal conductivity and the double diffusion process' ability to drive convective currents.The effects of magnetic fields, Soret, and Dufour are taken into consideration also the impacts of thermophoresis and Brownian motion, which are both crucial factors. Convergence of solutions obtained by use of the finite element technique is checked by plots and numerical data and they are assessed for a number of physical components that are involved in the problem and the obtained results are found good agreement with the previous one. Surface drag coefficient and local Nussult and Sherwood numbers are also studied through numerical values.

2 Methodology:

The fluid flow geometry of "steady, chemically reacting, viscous, incompressible, two-dimensional, electrically conducting, Oldroyd-B + Nanofluid and nanoparticles towards a porous stretching sheet in the presence of Magnetic field, Thermal diffusion, Thermophoresis, Diffusion thermo, and Brownian motion effects" is shown in Figure 1. For this investigation, the following assumptions are

i. The non-linearly stretching sheet is stretched along the x-direction and the y-axis is normal to it.

ii. In the domain y > 0, the Oldroyd-B + Nanofluid flow is occupied.

iii. It is assumed that the convective surface temperature is T_w and ambient temperature is T_∞. and the concentration of the nano-particles on the sheet is C_w and ambient concentration is C_∞.

iv. Generally, B(x) a variable magnetic field will be provided to the surface of the sheet while the magnetic field induced is minimal and may be justified for MHD flow at the small magnetic Reynolds number.

v. In addition, it is assumed that the effect described by Fourier's and Fick's law is of a higher order of magnitude than the effect due to Dufour and Soret, and thus the Dufour and Soret effects are considered.

vi. Homogeneous first-order chemical reaction is considered, and thermal radiation is neglected in this flow.

vii. Along the x-direction, the velocity of the sheet is $u_w(x) = ax$

y, v, η

Based on the above assumptions, the fundamental governing equations for the conservations of mass, momentum, energy, and concentration for the Oldroyd-B + Nanofluid are considered as:

Continuity Equation:

$$\left(\frac{\partial u}{\partial x}\right) + \left(\frac{\partial v}{\partial y}\right) = 0 \tag{1}$$

Momentum Equation:

$$u\left(\frac{\partial u}{\partial x}\right) + v\left(\frac{\partial u}{\partial y}\right) + \lambda_1\left(u^2\frac{\partial^2 u}{\partial x^2} + v^2\frac{\partial^2 u}{\partial y^2} + 2uv\frac{\partial^2 u}{\partial x\partial y}\right) =$$

$$\nu\left(\frac{\partial^2 u}{\partial y^2} + \lambda_2\left(-\frac{\partial u}{\partial x}.\frac{\partial^2 u}{\partial y^2} + v\frac{\partial^3 u}{\partial y^3} + u\frac{\partial^3 u}{\partial x\partial y^2} - \frac{\partial u}{\partial y}\frac{\partial^2 v}{\partial y^2}\right)\right\} - \left(\frac{\sigma B_o^2}{\rho}\right)u - \left(\frac{\nu}{k^*}\right)u, \tag{2}$$

Equation of thermal energy:

$$u\frac{\partial T}{\partial x} + v\frac{\partial T}{\partial y} = \alpha\left(\frac{\partial^2 T}{\partial y^2}\right) + \tau_B\left(D_B\left(\frac{\partial C}{\partial y}\frac{\partial T}{\partial y}\right] + \frac{D_T}{T_\infty}\left(\frac{\partial T}{\partial y}\right)^2\right\} + \frac{D_m K_T}{C_s C_p}\left(\frac{\partial^2 C}{\partial y^2}\right) \tag{3}$$

Equation of species nanoparticle volume concentration:

$$u\left(\frac{\partial C}{\partial x}\right) + v\left(\frac{\partial C}{\partial y}\right) = D_B\left(\frac{\partial^2 C}{\partial y^2}\right) + \frac{D_T}{T_\infty}\left(\frac{\partial^2 T}{\partial y^2}\right) + \frac{D_m K_T}{T_m}\left(\frac{\partial^2 T}{\partial y^2}\right) - Kr(C - C_\infty) \tag{4}$$

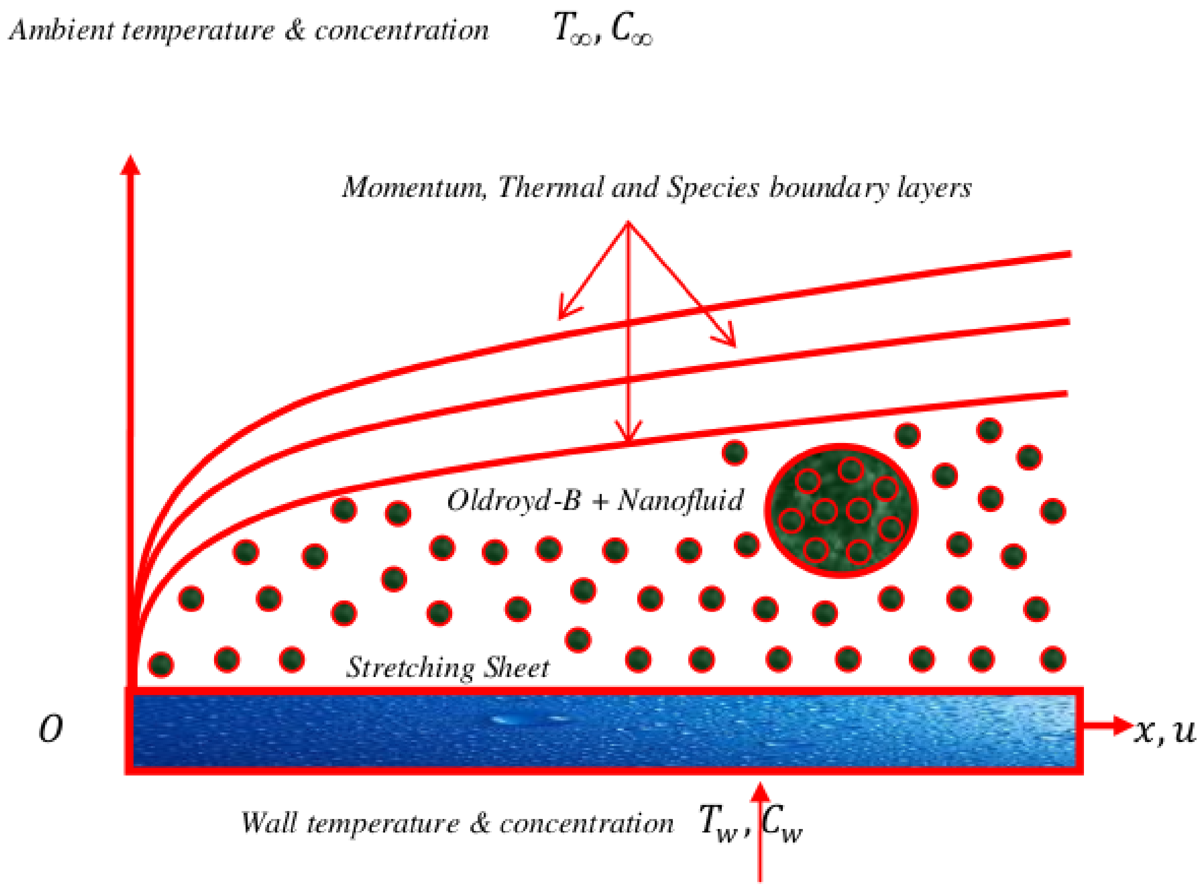

Fig 1. Geometry representation of the fluid

The boundary conditions for this flow are

$$\left.\begin{array}{l} u = u_w = ax, v = 0, T = T_w, C = C_w, \text{ at} y = 0 \\ u \to 0, T \to T_\infty, C \to C_\infty, \text{ as} y \to \infty \end{array}\right\} \tag{5}$$

Introducing the following similarity transformations

$$\left(u = axf'(\eta), v = -\sqrt{\nu a} f(\eta), \eta = y\sqrt{\frac{a}{\nu}}, \theta = \frac{T - T_\infty}{T_w - T_\infty}, \phi = \frac{C - C_\infty}{C_w - C_\infty}, \psi = xf(\eta)\sqrt{a\nu}, \right\} \tag{6}$$

where $\psi(x,y)$represents the stream function and is defined as
$u = \frac{\partial \psi}{\partial y}$ and $v = -\frac{\partial \psi}{\partial x}$ (7)

Making use of Eq. (7), equation of continuity is identically satisfied and Eqs. (2), (3) and (4) along with (5) take the following form

$$f''' + \gamma_1\left(f'^2 - ff'''\right) - Mf' - Kf' - f'^2 + ff'' - \gamma_2\left(f^2 f''' - 2ff' f''\right) = 0 \tag{8}$$

$$NbLe\theta'' + LeNbPrf\theta' + PrNbNt\theta'\phi' + PrNt\theta'^2 + PrLeNbDu\phi'' = 0 \tag{9}$$

$$Nb\phi'' + ScNbf\phi' + ScNt\theta'' + ScNbSr\theta'' - ScNb\delta\phi = 0 \tag{10}$$

the corresponding boundary conditions (5) become

$$\left(f(0)=0, f'(0)=1, \theta(0)=1, \phi(0)=1 \& f'(\infty)\to 0, \theta(\infty)\to 0, \phi(\infty)\to 0\right\} \tag{11}$$

where the involved physical parameters are defined as

$$\left.\begin{array}{l} M=\dfrac{\sigma B_o^2}{a\rho}, \Pr=\dfrac{v}{\alpha}, Le=\dfrac{\alpha}{D_B}, Nb=\dfrac{(\rho C)_p D_B T_\infty (C_w-C_\infty)}{D_T (T_w-T_\infty)}, \gamma_2=\lambda_2 C \\ K=\dfrac{v}{ak^*}, \gamma_1=\lambda_1 C, Sr=\dfrac{D_m K_T (T_w-T_\infty)}{T_m v(C_w-C_\infty)}, Du=\dfrac{D_m K_T (C_w-C_\infty)}{C_s C_p v(T-T_\infty)}, Sc=\dfrac{v}{D_B} \\ Nt=\dfrac{(\rho C)_p (C_w-C_\infty)}{(\rho C)_f}, Re_x=\dfrac{u_w x}{v}, \delta=\dfrac{Kr}{a}, \end{array}\right\} \tag{12}$$

Quantities of physical interest, the physical parameters of the skin-friction coefficient, local Nusselt number and local Sherwood number are presented as follows:

$$Cf=\left(\frac{1+\gamma_2}{1+\gamma_1}\right)\frac{\tau_w}{\rho u_w^2}=\left(\frac{1+\gamma_2}{1+\gamma_1}\right)\frac{\mu}{\rho u_w^2}\left(\frac{\partial u}{\partial y}\right)_{y=0} \Rightarrow \left(\sqrt{Re_x}\right)Cf=\left(\frac{1+\gamma_2}{1+\gamma_1}\right)f''(0) \tag{13}$$

$Nu_x=\frac{xq_w}{\kappa(T_w-T_\infty)}$ where $q_w=-\kappa\left(\frac{\partial T}{\partial y}\right)_{y=0} \Rightarrow Nu=Re_x^{-\frac{1}{2}}Nu_x=-\theta'(0)$ (14)

$Sh_x=\frac{xq_m}{D_B(T_w-T_\infty)}$ where $q_m=-D_B\left(\frac{\partial C}{\partial y}\right)_{y=0} \Rightarrow Sh=Re_x^{-\frac{1}{2}}Sh_x=-\phi'(0)$ (15)

2.1 Finite Element Method Solutions:

Use the finite element method to solve both partial and ordinary differential equations. This is a very good way to solve differential equations. As we've already said, the finite element method is based on the idea that the domain can be broken up into smaller, finite-dimensional units called finite elements. At the time this was written, this was the most flexible numerical method for engineering analysis. It has been used to study a wide range of things, such as heat transfer, fluid mechanics, rigid body dynamics, solid mechanics, chemical reactions, electrical systems, and acoustics, to name a few. Before doing a finite element analysis, the following steps must be taken:

- **Domain discretization into elements:** Using finite element discretization, the whole interval is broken up into a certain number of smaller intervals, each of which is called an element.
- **Domain decomposition into elements:** The finite-element mesh is made up of all of the elements that were previously mentioned.
- To generate element equations, the following technique should be followed:
  - Initial variations of the mathematical model are made over the typical element (a single element from the mesh).
  - When the variational problem has an approximate solution, the element equations are constructed by substituting the estimated solution into the previously established system, which is then solved for the variable.
  - This matrix is formed by interpolating polynomials and is referred to as a stiffness matrix.
- **Putting together and solving equations:** All algebraic equations must be constructed by placing restrictions on each equation's constituents regarding inter-element continuity. By tying a lot of algebraic equations together, it is feasible to create a global finite-element model of the whole domain.
- **Imposition of boundary conditions:** It is important to apply the boundary conditions of the flow model to the created equations.

Built equations may be solved using a variety of numerical approaches, including the LU decomposition method, the Gauss elimination method, and others. When working with real numbers, it is essential to remember the form functions used to approximate real functions. There are a total of 20,001 nodes in the flow domain, which is partitioned into 10,000 similarly sized quadratic components. The flow domain is made up of 10,000 similar-sized quadratic components. After creating the element equations, we were provided with 80,004 nonlinear equations for analysis. After applying the boundary conditions, the remaining system of nonlinear equations is solved numerically using the Gauss elimination technique with a precision of 0.00001. The use of Gaussian quadrature facilitates the solution of integrations.

Table 1. Comparison of present Nusselt number results with published results

Pr	Khan and Pop [25]	Present Nusselt results
0.07	0.066	0.06546736076092640923
0.20	0.169	0.16573676376209468757
0.70	0.454	0.44987609763434709643
2.00	0.911	0.90850763049630946134

2.2 Program Code Validation:

To check the accuracy of computed results in this paper via finite element method, a comparison of numerical values of Nusselt number results are made for several values of Prandtl number Pr. To do this, the attained numerical results which are approved against the consequences of Khan and Pop [25] as presented in Table 1. It is observed that numerical results of present analysis are found in good agreement.

3 Results and Discussion:

This study investigates the mathematical analysis of the impact of diffusion-thermo and thermo-diffusion on the flow of Oldroyd-B + Nanofluid MHD through a permeable medium on a stretched sheet. The study considers the impacts of chemical reaction, thermophoresis, and Brownian motion. The finite difference technique is used to get solutions. The flow regime experiences significant Soret and Dufour effects, along with chemical reactions, due to density fluctuations. Both the Soret and Dufour effects may play a significant role when species with a different density than the surrounding fluid are introduced at the surface of a fluid field. Velocity, temperature and concentration profiles are shown in Figure 2 to Figure 15 for different values of various parameters. It is unchanging M = 0.5, K = 0.5, γ_1 = 0.5, γ_2 = 0.5, Pr = 0.71, Nb = 0.3, Nt = 0.1, Du = 0.5, Le = 0.3, Sc = 0.22, Sr = 0.5 and δ = 0.5. Figure 2 illustrates the connection in velocity for magnetic field parameter (M) values. The rise in M has been shown to reduce velocity. As M elevates, a resistive force similar to a drag force is generated, which is known as Lorentz force. The velocity intensity is retarded by the Lorentz force, which decelerates its motion. The graph in Figure 3 shows that the fluid-flow resistive force decreases with the rise in the porosity parameter or permeability parameter (K), i.e. when the porosity parameter increases, resulting in increased velocity of fluid-flow and also the flow behavior of Oldroyd-B nanofluids is greatly influenced by the permeability of a porous medium, particularly in applications such as heat exchangers, filtration, and geothermal energy extraction. Both viscous and elastic components are included in the Oldroyd-B model to account for non-Newtonian fluid properties, which get more complicated as the fluid passes through a porous material. A more readily flowable nanofluid is produced when the permeability of the porous media rises and the flow resistance falls. Because the fluid may pass through the pores more easily, larger flow rates and better heat transfer performance are made possible. In these situations, the system transfers heat more effectively because the nanoparticles in the nanofluid improve thermal conductivity.Nonetheless, flow is increased by a decreased permeability, which is usually present in materials with fine pores or dense packing. Figure 4 shows the influence of the Deborah number (γ_1) on the velocity profiles. By increasing γ_1,the fluid velocity increases. This is due to fact that γ_1 involves relaxation time. An increase in the relaxation time leads to increase in the temperature and boundary layer thickness. Figure 5 illustrates the effects of the Deborah number (γ_2) on the velocity field. From this figure, it is noted that the behavior of the γ_2 is opposite to that of γ_1. This is due to fact that the retardation time provides resistance which causes a reduction in the velocity and thermal boundary layer thickness. A demonstration of the variability in temperature profiles is provided by the Prandtl number Pr, which is computed from the data shown in Figure 6. A link has been seen between dropping Pr values and a matching decline in temperature profiles. This association has been demonstrated and observed. A lower Prandtl number in the fluid results in a greater heat transfer rate and a lower thermal diffusivity. This is the reason why this is the case. As a direct result of this condition, the thermal diffusivity of the fluid will decrease. When compared to fluids with a higher Prandtl number Pr, fluids with a lower Prandtl number Pr have a higher thermal conductivity, which results in the production of thermal boundary layer structures that are more substantial. The reason for this is because there is an inverse relationship between greater thermal conductivities and lower Prandtl values. The behavior of the dimensionless temperature and concentration curves is seen in Figures 7 and 8, respectively, when the Brownian motion parameter, which is indicated by the symbol Nb, is applied. A decrease in the concentration profiles and an increase in the temperature profiles are seen when the Nb values are increased. When the values of the Brownian motion parameter are increased, turbulent motion is produced. This, in turn, causes the kinetic energy of the nanoparticles to increase, which in turn causes the temperature of the nanofluid to rise. The reason for the occurrence of this phenomenon is because chaotic motion displays expansion in a manner that is consistent with the principles of Brownian motion. See Figures 9 and 10 for an illustration of how the thermophoresis parameter

Nt has an effect on the temperature and concentration curves. An increase in the values of the thermophoresis parameters causes a concomitant rise in the temperature profile as well as the concentration profile respectively. In addition, the thickness of the border layer grows throughout this process. At its heart, this is brought about by a phenomenon that is referred to as thermophoresis. This phenomenon takes place when there is a considerable temperature differential between the sheet and the fluid. The behavior of the Dufour number (Du) and the Soret number (Sr) with regard to temperature and concentration profiles is shown in Figures 11 and 12, respectively. Each of these figures is shown in sequential order. After doing an analysis of this image, we discovered that increasing the value of Du resulted in a commensurate increase in the thermal layer's thickness as well as its temperature. A concentration gradient has a direct impact on the amount of heat energy that is contained inside a liquid, which in turn has an effect on Du. Increasing Sr values also sharpen concentration profiles, in a way that is comparable to the impact that is caused by increasing Sr levels. When a temperature gradient is present, it makes it easier for mass to flow from a location with a lower concentration of solutes to a region with a higher concentration of solutes. According to the data shown in Figure 13, a rise in the Lewis number (Le) results in a decrease in the temperature as well as the thickness of the thermal boundary layer. Presented in Figure 14 is an illustration of the impact that the Schmidt number (Sc) has on dimensionless concentration patterns. A drop in concentration has been shown to occur whenever there is an increase in the Schmidt number (Sc). A visual representation of the influence of the chemical reaction (δ) on the concentration profile may be shown in Figure 15. It has been shown that the concentration experiences a decline as the intensity of the chemical reaction increases.

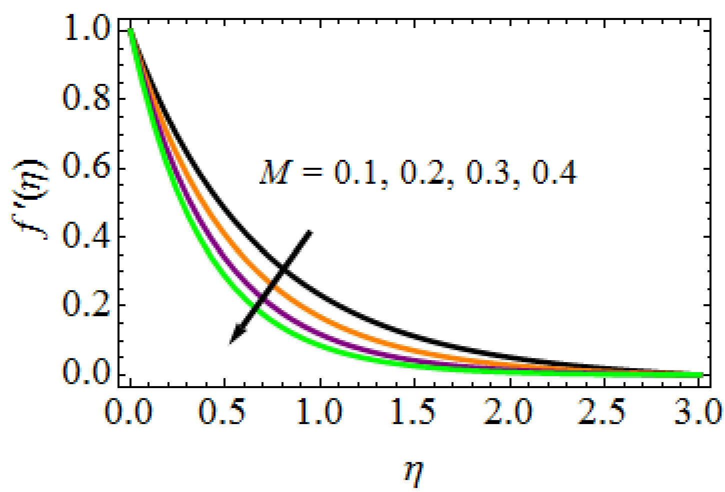

Fig 2. M influence on velocity profiles

Table 2 shows the numerical data of Skin-friction $\left(\frac{1+\gamma_2}{1+\gamma_1}\right) f''(0)$coefficient for changes of M, K, γ_1, γ_2, Pr, Le, Nb, Nt, Sr, Du, Sc and δ. From this table, the Skin-friction $\left(\frac{1+\gamma_2}{1+\gamma_1}\right) f''(0)$coefficient increases with increasing values of γ_1, Nb, Nt, Sr, Du, while it decreases with increasing values of M, K, γ_2, Pr, Le, Sc and δ. The numerical results of Nusselt number $\left(-\theta'(0)\right)$ in terms of Nusselt number for different values of Pr, Le, Nb, Nt, and Du, are presented in Table 3. From this table, it is observed that the heat transfer rate is rising with growing values of Nb, Nt, Du, while it reduces for increasing values of Pr and Le. Rate of mass transfer $\left(-\phi'(0)\right)$ in terms of Sherwood number for variations of Nb, Nt, Sr, Sc and δ are presented in Table 4. From this table, it is noticed that Sherwood number $\left(-\phi'(0)\right)$ is growing with higher values of Nt, and Sr, and the reverse effect is observed in the case of increasing values of Le, Nb and δ.

4 Conclusion

The study presents the flow of a two-dimensional, steady, incompressible, viscous, electrically conducting, chemically reacting Oldroyd-B + nanofluid through a porous medium in close proximity to a stretching sheet that is surrounded by porous medium while being subjected to the influence of a magnetic field. The study also investigated the combined effects of thermal diffusion and diffusion thermo on the flow of the nanofluid. The following are important conclusion-derived conclusions.

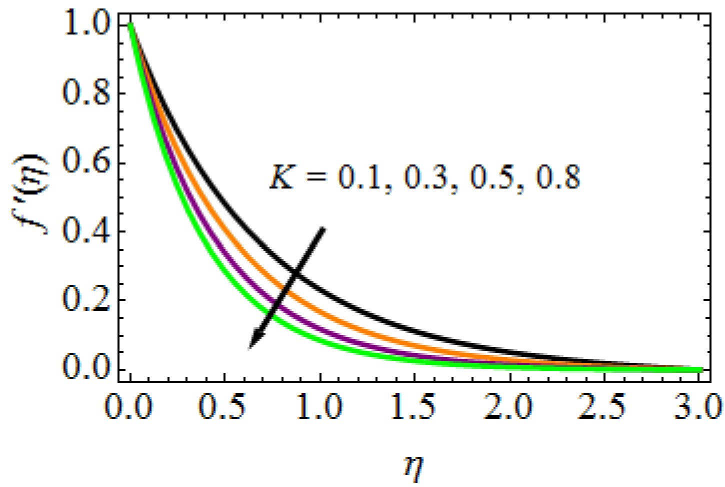

Fig 3. K influence on velocity profiles

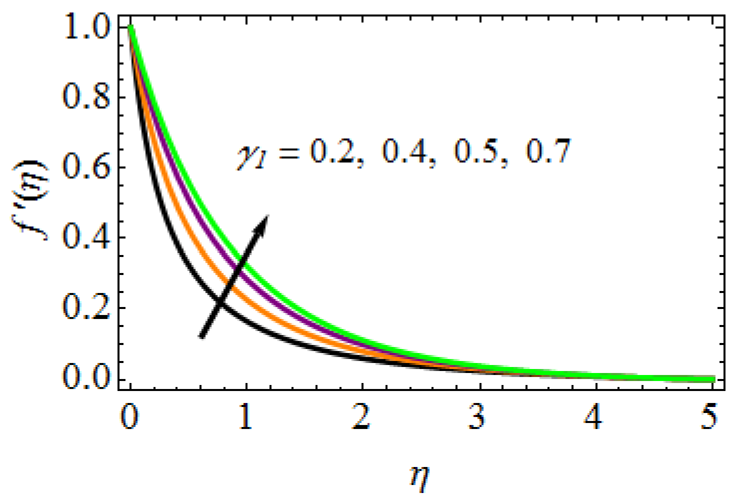

Fig 4. γ_1 influence on velocity profiles

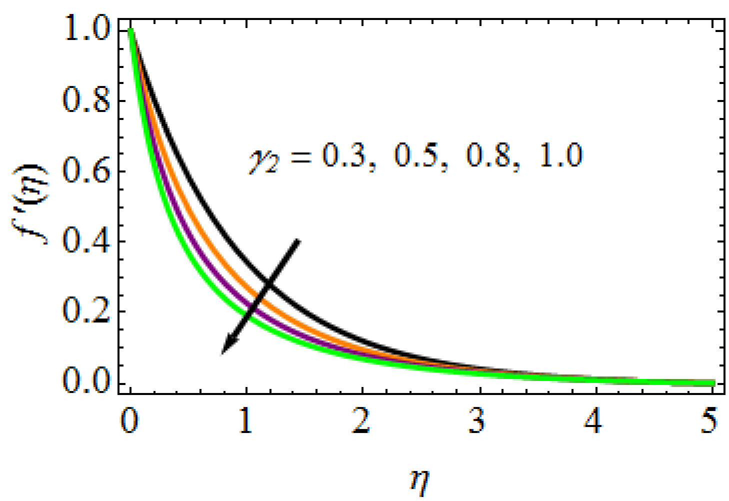

Fig 5. γ_2 influence on velocity profiles

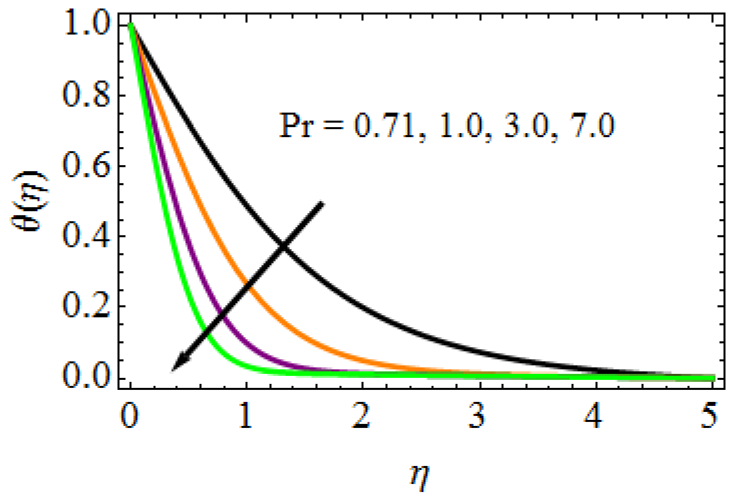

Fig 6. *Pr* influence on temperature profiles

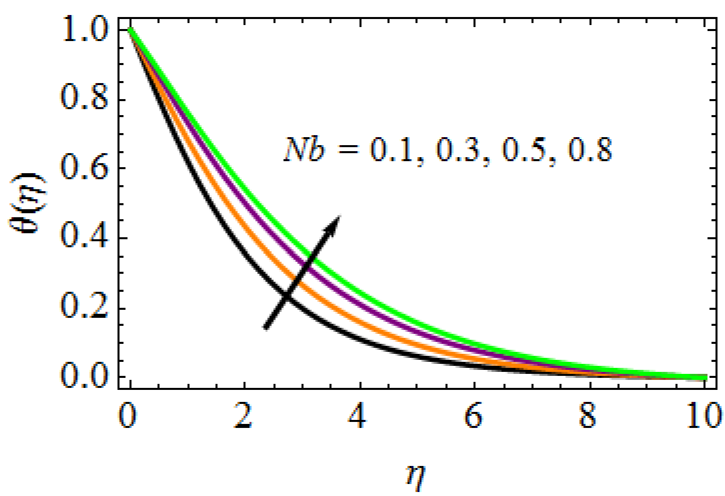

Fig 7. *Nb* influence on temperature profiles

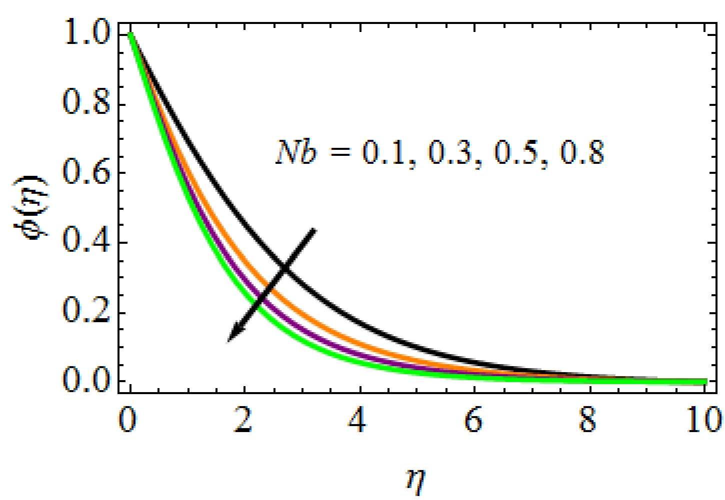

Fig 8. *Nb* influence on concentration profiles

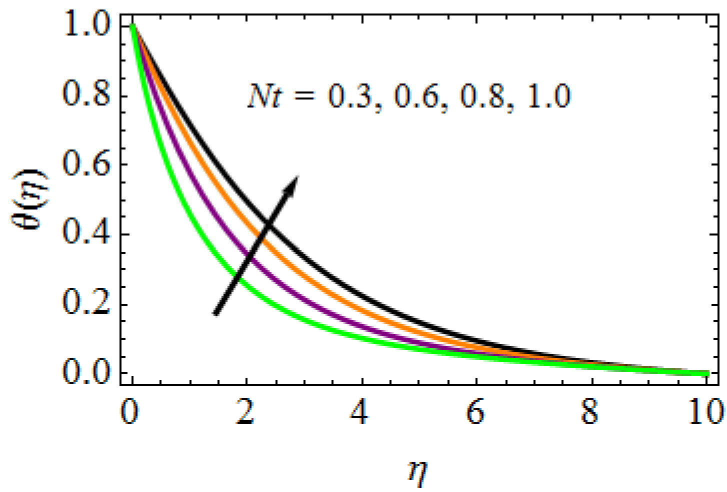

Fig 9. *Nt* influence on temperature profiles

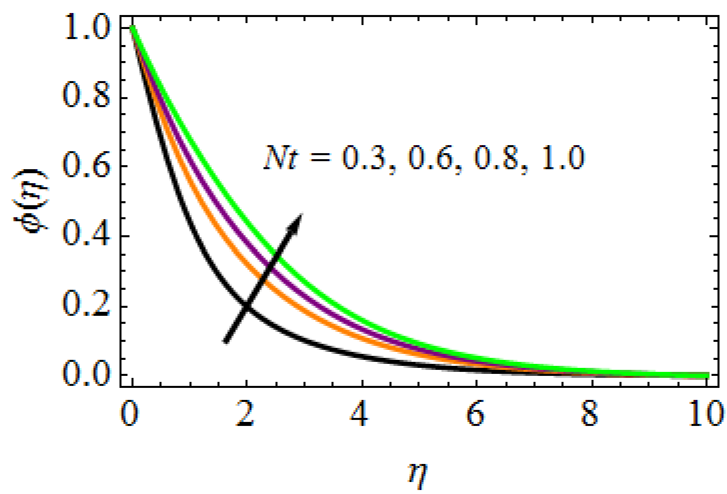

Fig 10. *Nt* influence on concentration profiles

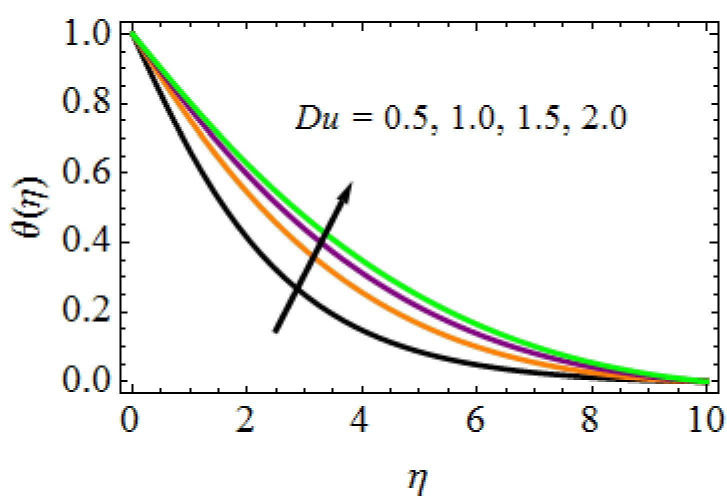

Fig 11. *Du* influence on temperature profiles

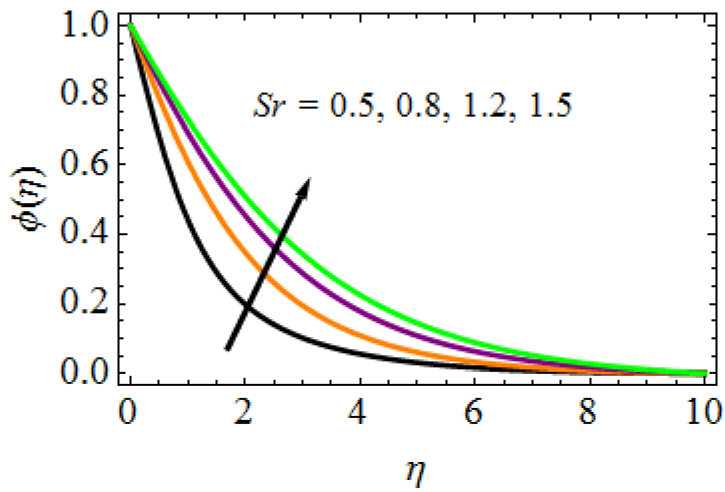

Fig 12. *Sr* influence on concentration profiles

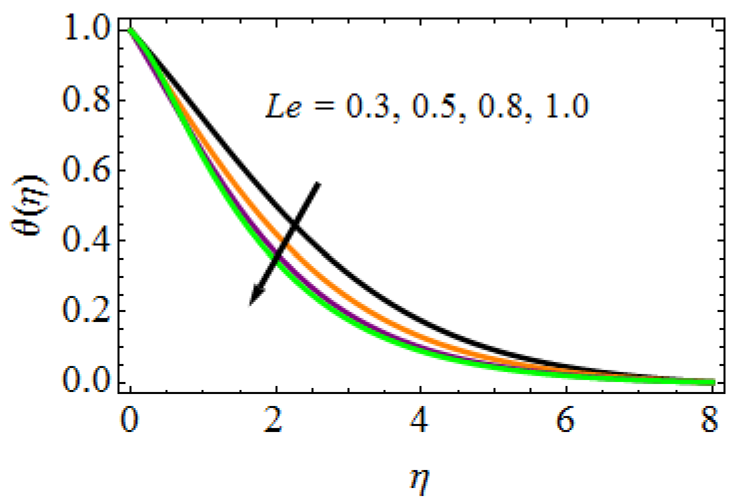

Fig 13. *Le* influence on temperature profiles

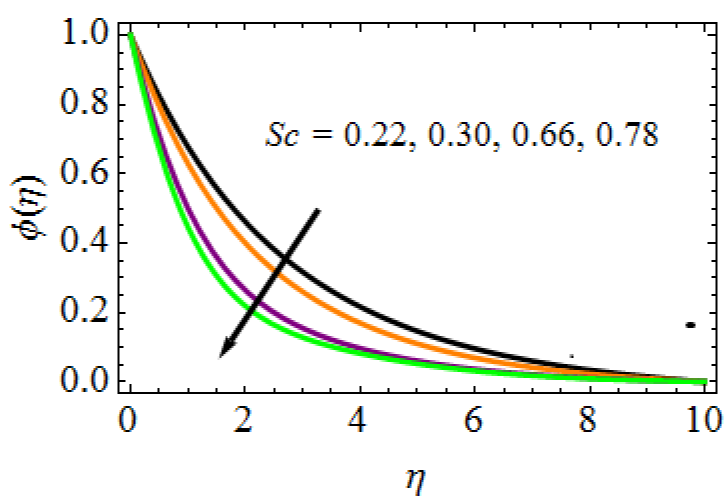

Fig 14. *Sc* influence on concentration profiles

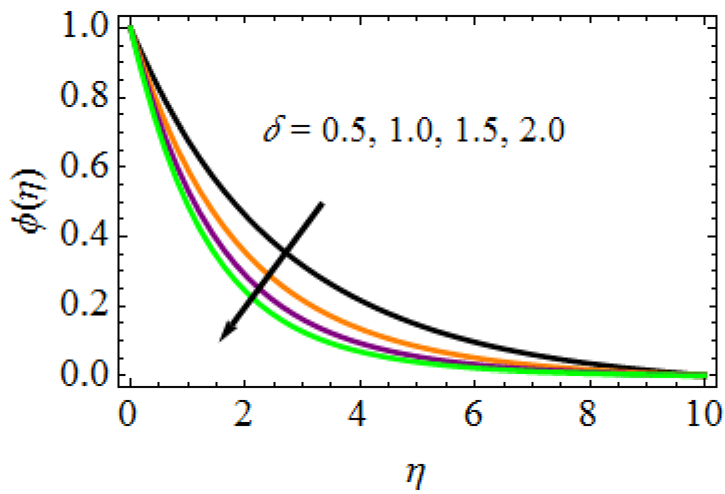

Fig 15. γ influence on concentration profiles

Table 2. Numerical values of Skin-friction coefficient for variations of M, K, γ_1, γ_2, Pr, Le, Nb, Nt, Sr, Du, Sc and δ

M	K	γ_1	γ_2	Pr	Le	Nb	Nt	Sr	Du	Sc	δ	$\left(\frac{1+\gamma_2}{1+\gamma_1}\right) f''(0)$
0.1	0.1	0.2	0.3	0.71	0.3	0.1	0.3	0.5	0.5	0.22	0.5	1.56861987945
0.2												1.51807034963
0.3												1.49198795874
	0.3											1.53083671341
	0.5											1.51697364093
		0.4										1.59876503034
		0.5										1.62098748572
			0.5									1.54673064713
			0.8									1.52156740844
				1.00								1.51876630936
				7.00								1.49098298709
					0.5							1.53763876303
					0.8							1.51153456349
						0.3						1.58678679063
						0.5						1.60769187893
							0.6					1.59878317934
							0.8					1.62134721659
								0.8				1.58084718797
								1.2				1.61676836971
									1.0			1.59156087360
									1.5			1.62760978334
										0.30		1.52673647304
										0.66		1.48678798278
											1.0	1.52234877865
											1.5	1.50080802426

Table 3. $-\theta^{'}(0)$ numerical values for variations of Pr, Le, Nb, Nt and Du

Pr	Le	Nb	Nt	Du	$-\theta^{'}(0)$
0.71	0.3	0.1	0.3	0.5	0.86876093034
1.00					0.84730467095
7.00					0.82768715745
	0.5				0.82678457360
	0.8				0.79679802854
		0.3			0.89576873480
		0.5			0.91657606134
			0.6		0.90346587045
			0.8		0.92789609526
				0.8	0.89567650735
				1.2	0.91867015609

Table 4. $-\phi^{'}(0)$ numerical values for variations of Nb, Nt, Sr, Sc and δ

Nb	Nt	Sr	Sc	δ	$-\phi^{'}(0)$
0.1	0.3	0.5	0.22	0.5	1.10697968133
0.3					1.05756017526
0.5					1.00665790591
	0.6				1.13013560946
	0.8				1.16176076334
		0.8			1.12460736076
		1.2			1.15786508765
			0.30		1.02676827003
			0.66		0.98476087634
				1.0	1.06576036453
				1.5	1.03866927965

- Velocity profile shows reduction due to an increase in magnetic field due to Lorentz forces are big reason behind the resistance in motion of fluid particles.
- The velocity profiles falls down for variations of γ_2 and the reverse effect is observed in the case of γ_1.
- The velocity profiles decrease with increasing values of the Porous medium parameter.
- Prandtl number shows the reduction in temperature due to the inverse relation of Prandtl number and thermal diffusivity.
- By increasing the Thermophoresis parameter, the temperature increases and the nanoparticle volume concentration increases as the Thermophoresis parameter increases.
- Through increasing the Brownian motion parameter, the temperature increases and the nanoparticle volume concentration decreases.
- As Schmidt number increases, the nanoparticle volume concentration decreases.
- The continuous values of the Chemical reaction parameter δ serve to diminish the profiles of concentration.

5 Nomenclature:

List of Symbols:

u, v: Velocity components in $x$and $y$axes respectively (m/s)
x, y: Cartesian coordinates measured along the stretching sheet (m)
f: Dimensionless stream function
$f^{'}$: Fluid velocity (m/s)
Pr: Prandtl number
C: Fluid concentration (mol/m^3)
C_∞: Dimensional ambient volume fraction (mol/m^3)

T: Fluid temperature (K)
Cf: Skin-friction coefficient
T_∞: Temperature of the fluid far away from the stretching sheet (K)
M: Magnetic field parameter
B_o: Uniform magnetic field
Le: Lewis number
C_w: Dimensional concentration at the stretching surface (mol/m^3)
Nu: Rate of heat transfer coefficient (or) Nusselt number
Sh: Rate of mass transfer coefficient (or) Sherwood number
C_p: Specific heat capacity of nanoparticle material
Nb: Brownian Motion parameter
Nt: Thermophoresis parameter
D_B: Brownian diffusion coefficient
D_T: Thermophoresis diffusion coefficient
a: Positive real number
u_w: Stretching velocity of the fluid along x - direction (m/s)
Du: Diffusion thermo (or) Dufour number
Sr: Thermal diffusion (or) Soret number
C_s: Concentration susceptibility
K_T: Thermal diffusion ratio
D_m: Solutal diffusivity of the medium
T_m: Fluid Mean temperature
O: Origin
q_w: Heat flux coefficient
q_m: Mass flux coefficient
Re_x: Reynold's number
k^*: Dimensional permeability parameter
K: Permeability parameter
Kr: Dimensional chemical reaction
Sc: Schmidt number
T_m: Fluid mean temperature

Greek symbols:

η: Dimensionless similarity variable
θ: Dimensionless temperature (K)
α: Nanofluid thermal diffusivity (m^2/s)
ν: Kinematic viscosity (m^2/s)
φ: Dimensionless nanofluid concentration (mol/m^3)
ρ: Density of the fluid
σ: Electrical Conductivity
μ: Dynamic viscosity of the fluid, (Pascal-second)
κ: Thermal conductivity of the fluid, (W / (m· K))
γ_1: Deborah number for relaxation time
γ_2: Deborah number for retardation time
λ_1: Relaxation time
λ_2: Retardation time
τ_w: Shear stress
ψ: Stream function
δ: Chemical reaction parameter

Superscript:
$/$**:** Differentiation w.r.t η
Subscripts:
f**:** Fluid
w**:** Condition on the sheet
∞**:** Ambient Conditions

References

1) Hussain A, Haider Q, Rehman A, Malik MY, Nadeem S, Hussain S. Heat transport improvement and three-dimensional rotating cone flow of hybrid-based nanofluid. *Math Probl Eng*. 2021. doi:10.1155/2021/6633468.
2) Li S, Puneeth V, Saeed AM, Singhal A, Al-Yarimi FA, Khan MI, et al. Analysis of the Thomson and Troian velocity slip for the flow of ternary nanofluid past a stretching sheet. *Sci Rep*. 2023;13(1):2340–2340. doi:10.1038/s41598-023-29485-0.
3) Thejas R, Naveen CS, Khan MI, Prasanna GD, Reddy S, Oreijah M, et al. A review on electrical and gas-sensing properties of reduced graphene oxide-metal oxide nanocomposites. *Biomass Convers Biorefinery*. 2022;p. 1–11. doi:http://dx.doi.org/10.1007/s13399-022-03258-7.
4) Ahmed K, Akbar T. Numerical investigation of magnetohydrodynamics Williamson nanofluid flow over an exponentially stretching surface. *Adv Mech Eng*. 2021;13(5). doi:http://dx.doi.org/10.1177/16878140211019875.
5) Aly EH. Dual exact solutions of graphene-water nanofluid flow over stretching/shrinking sheet with suction/injection and heat source/sink: critical values and regions with stability. *Powder Technol*. 2019;342:528–544. doi:10.1016/j.powtec.2018.09.093.
6) Hussanan A, Qasim M, Chen ZM. Heat transfer enhancement in sodium alginate based magnetic and non-magnetic nanoparticles mixture hybrid nanofluid. *Phys Stat Mech Appl*. 2020;550. doi:10.1016/j.physa.2019.123957.
7) Khan A, Shah Z, Alzahrani E, Islam S. Entropy generation and thermal analysis for rotary motion of hydromagnetic Casson nanofluid past a rotating cylinder with Joule heating effect. *Int Commun Heat Mass Transfer*. 2020;119:104979–104979. doi:10.1016/j.icheatmasstransfer.2020.104979.
8) Khan AS, Nie Y, Shah Z, Dawar A, Khan W, Islam S. Three-dimensional nanofluid flow with heat and mass transfer analysis over a linear stretching surface with convective boundary conditions. *Appl Sci*. 2018;8(11):2244–2244. doi:10.3390/app8112244.
9) Manna NK, Biswas N, Mandal DK, Sarkar UK, Öztop HF, Abu-Hamdeh N. Impacts of heater-cooler position and Lorentz force on heat transfer and entropy generation of hybrid nanofluid convection in quarter-circular cavity. *Int J Numer Meth Heat Fluid Flow*. 2023;33(3):1249–1286. doi:10.1108/hff-07-2022-0402.
10) Waqas H, Imran M, Hussain S, Ahmad F, Khan I, Nisar KS, et al. Numerical simulation for bioconvection effects on MHD flow of Oldroyd-B nanofluids in a rotating frame stretching horizontally. *Math Comput Simul*. 2020;178:166–182. doi:http://dx.doi.org/10.1016/j.matcom.2020.05.030.
11) Waqas H, Farooq U, Naseem R, Hussain S, Alghamdi M. Impact of MHD radiative flow of hybrid nanofluid over a rotating disk, Case Stud. *Therm Eng*. 2021;26:101015–101015. doi:10.1016/j.csite.2021.101015.
12) Lu DC, Farooq U, Hayat T, Rashidi MM, Ramzan M. Computational analysis of three layer fluid model including a nanomaterial layer. *Int J Heat Mass Transf*. 2018;122:222–228. doi:10.1016/j.ijheatmasstransfer.2018.01.080.
13) Rajeev A, Manjunatha S, Puneeth V, Khan MI. Analogy of cross-diffusion in sinusoidal channel for the flow of micropolar hybrid nanofluid sandwiched between single-phase nanofluid in a three-layer model. *Waves Random Complex Media (2023)*;p. 1–23. doi:10.1080/17455030.2023.2194447.
14) Abbasi FM, Shanakhat I, Shehzad SA. Analysis of entropy generation in peristaltic nanofluid flow with Ohmic heating and Hall current. *Phys Scripta*. 2019;94(2). doi:10.1088/1402-4896/aaf600.
15) Ma X, Song Y, Wang Y, Zhang Y, Xu J, Yao S, et al. Experimental study of boiling heat transfer for a novel type of GNP-Fe3O4 hybrid nanofluids blended with different nanoparticles. *Powder Technol*. 2022;396:92–112. doi:10.1016/j.powtec.2021.10.029.
16) Gangadhar K, Lakshmi KB, Kannan T, Chamkha AJ. Bio-convective magnetized Oldroyd-B nanofluid flow in the presence of Joule heating with gyrotactic microorganisms. *Waves Random Complex Media (2022)*;p. 1–21. doi:10.1080/17455030.2022.2050441.
17) Rafiq M, Yasmin H, Hayat T, Alsaadi F. Effect of Hall and ion-slip on the peristaltic transport of nanofluid: a biomedical application. *Chin J Phys*. 2019;60:208–227. doi:10.1016/j.cjph.2019.04.016.
18) Hina S, Kayani SM, Mustafa M. Aiding or Opposing Electro-Osmotic Flow of Carreau-Yasuda Nanofluid Induced by Peristaltic Waves Using Buongiorno Model. *Waves in Random and Complex Media (2022)*;p. 1–17. doi:10.1080/17455030.2021.2024299.
19) Tanveer A, Malik MY. Slip and porosity effects on peristalsis of MHD Ree-Eyring nanofluid in curved geometry. *Ain Shams Eng J*. 2021;12(1):955–968. doi:10.1016/j.asej.2020.04.008.
20) Rafiq M, Sajid M, Alhazmi SE, Khan MI, El-Zahar ER. MHD electroosmotic peristaltic flow of Jeffrey nanofluid with slip conditions and chemical reaction. *Alex Eng J*. 2022;61(12):9977–9992. doi:10.1016/j.aej.2022.03.035.
21) Dang K, Makkar V, Sharma N. Mathematical Simulation for MHD Casson Convective Nanofluid Flow Induced by 3D Permeable Sheet with Chemical Effect. *Indian Journal of Science and Technology*. 2024;17(16):1713–1723. doi:10.17485/IJST/v17i16.117.
22) Dang K, Makkar V, Sharma N. Radiative MHD Casson Non-Newtonian Nanofluid Slip Flow Induced by Stretching Cylinder: A Numerical Approach. *Indian Journal of Science and Technology*. 2024;17(38):3993–4004. doi:10.17485/IJST/v17i38.1978.
23) Dadheech A, Sharma S, Al-Mdallal Q. Numerical simulation for MHD Oldroyd-B fluid flow with melting and slip effect. *Sci Rep*. 2024;14:10591–10591. doi:10.1038/s41598-024-58376-1.
24) Haider A, Anwar MS, Nie Y, Alqarni MS. Enhanced heat and mass transfer in porous media with Oldroyd-B complex nano-fluid flow and heat source. *Computers & Mathematics with Applications*. 2024;170. doi:10.1016/j.camwa.2024.07.014.
25) Khan WA, Pop I. Boundary-layer flow of a nanofluid past a stretching sheet. *Int J Heat Mass Transf*. 2010;53:2477–2483. doi:10.1016/j.ijheatmasstransfer.2010.01.032.